

Unexpected radial and out-of-plane spin texture in the giant Rashba semiconductor BiTeI

Bo Liang(梁波), Jie Pang(庞杰), Neng Cai(蔡能), Wenpei Zhu(朱文培), Cheng Zhang(张成), Koji Miyamoto, Taichi Okuda, Kenya Shimada, Shilong Wu(吴仕龙), Lin Zhao(赵林), Youguo Shi(石友国), X. J. Zhou(周兴江), Guodong Liu(刘国东)

Citation: Chin. Phys. B. 35, 097902 (2026). DOI: 10.1088/1674-1056/ae7260 |
CSTR: 32038.14.CPB.ae7260
http://cpb.iphy.ac.cn; http://iopscience.iop.org/cpb

What follows is a list of articles you may be interested in

Spin- and state-resolved charge transfer and excitation in low-energy He+–Na(3s,3p) collisions

Xiao-Xia Wang(王小霞), Rui Tang(唐瑞), Li Ma(马丽), Chuan-Yu Zhang(张传瑜), Jian-Guo Wang(王建国), Yi-Zhi Qu(屈一至)

Chin. Phys. B. 35, 073402 (2026). DOI: 10.1088/1674-1056/ae705c | CSTR: 32038.14.CPB.ae705c

Electronic structure and superconducting gap of HgBa2Ca2Cu3O8+δ revealed by laser-based angle-resolved photoemission spectroscopy

Taimin Miao(苗泰民), Wenshan Hong(洪文山), Qinghong Wang(汪清泓), Shanshan Zhang(张珊珊), Bo Liang(梁波), Wenpei Zhu(朱文培), Neng Cai(蔡能), Mingkai Xu(徐明楷), Shenjin Zhang(张申金), Fengfeng Zhang(张丰丰), Feng Yang(杨峰), Zhimin Wang(王志敏), Qinjun Peng(彭钦军), Zuyan Xu(许祖彦), Hanqing Mao(毛寒青), Zhihai Zhu(朱志海), Xintong Li(李昕彤), Guodong Liu(刘国东), Lin Zhao(赵林), Yuan Li(李源), X. J. Zhou(周兴江)

Chin. Phys. B. 35, 027402 (2026). DOI: 10.1088/1674-1056/ae23b1 | CSTR: 32038.14.CPB.ae23b1

Resolving gravitational redshift with sub-millimeter height differences using spin-squeezed optical clocks

Deshui Yu(于得水), Jia Zhang(张佳), Shougang Zhang(张首刚), Tiantian Shi(史田田), Jingbiao Chen(陈景标)

Chin. Phys. B. 34, 054208 (2025). DOI: 10.1088/1674-1056/adca1d | CSTR: 32038.14.CPB.adca1d

---

RAPID COMMUNICATION

Unexpected radial and out-of-plane spin texture in the giant Rashba semiconductor BiTeI

Bo Liang(梁波)[1,2,†], Jie Pang(庞杰)[1,2,†], Neng Cai(蔡能)[1,2], Wenpei Zhu(朱文培)[1,2], Cheng Zhang(张成)[3], Koji Miyamoto[3], Taichi Okuda[3,4,5], Kenya Shimada[3,4,5], Shilong Wu(吴仕龙)[6], Lin Zhao(赵林)[1,2,6], Youguo Shi(石友国)[1,2,6,‡], X. J. Zhou(周兴江)[1,2,6,§], and Guodong Liu(刘国东)[1,2,6,¶]

[1] *Beijing National Laboratory for Condensed Matter Physics, Institute of Physics, Chinese Academy of Sciences, Beijing* 100190, *China*
[2] *School of Physical Sciences, University of Chinese Academy of Sciences, Beijing* 100049, *China*
[3] *Research Institute for Synchrotron Radiation Science, Hiroshima University,* 739-0046 *Higashi-Hiroshima, Japan*
[4] *International Institute for Sustainability with Knotted Chiral Meta Matter, Hiroshima University, Higashi-Hiroshima, Hiroshima* 739-8526, *Japan*
[5] *Research Institute for Semiconductor Engineering,* 1-4-2 *Kagamiyama, Higashi-Hiroshima, Hiroshima* 739-8527, *Japan*
[6] *Songshan Lake Materials Laboratory, Dongguan* 523808, *China*

(Received 30 April 2026; revised manuscript received 25 May 2026; accepted manuscript online 25 May 2026)

BiTeI is a model bulk Rashba semiconductor, with the 3.85 eVÅ record-high Rashba parameter among any known materials. A standard Rashba picture features an in-plane chiral spin texture on a pair of concentric Fermi surfaces, with the strict spin–momentum locking of the quasiparticles. However, for the first time, here we observe the unconventional spin textures beyond classical Rashba physics in BiTeI using high-resolution spin- and angle-resolved photoemission spectroscopy with full 3D vectorial spin detection. By simultaneously resolving all three spin components (P_X, P_Y, and P_Z), we achieve a band-resolved determination of the complete three-dimensional spin-vector texture for both the inner and outer Rashba-split bands. While the tellurium-terminated surface largely preserves the canonical tangential spin texture, the Iodine-terminated surface exhibits pronounced radial and sizable out-of-plane spin components, resulting in an unusual spin configuration. These findings reveal that the spin texture in BiTeI can be fundamentally reconfigured by surface termination, establishing surface engineering as a powerful route to control spin textures beyond the ideal Rashba paradigm.

Keywords: spin-resolved angle-resolved photoemission spectroscopy (spin-ARPES)

PACS: 79.60.–i, 71.70.Ej, 73.20.At

DOI: 10.1088/1674-1056/ae7260 **CSTR:** 32038.14.CPB.ae7260

1. Introduction

BiTeI has drawn broad attention as a prototypical polar Rashba semiconductor in which strong spin–orbit coupling (SOC) and bulk inversion asymmetry cooperate to generate giant Rashba-type spin splitting. It exhibits one of the largest known bulk Rashba parameters, with $\alpha_R = 3.85\ \text{eV}\cdot\text{Å}$.[1] Owing to its layered non-centrosymmetric crystal structure, spin-split states have been observed in both bulk-derived and surface-confined electronic bands,[2–4] establishing BiTeI as a model platform for exploring spin–momentum locking and spin-dependent quantum phenomena. More recently, efficient spin–charge interconversion in BiTeI-based heterostructures,[5] spin–orbit-torque switching in magnetically doped BiTeI,[6] and tunable spin Hall responses[7] have highlighted the spintronic potential of BiTeI. In parallel, the exfoliation of single- and few-layer BiTeI flakes[8–11] and the nanoscale modulation of the Rashba energy by local defects[12] further establish BiTeI as a promising low-dimensional Rashba material for interfacial and device functionalities as well as nonlinear optical applications.[13,14] In the simplest Rashba picture,[15] the spin texture is expected to be purely tangential to the constant-energy contour (CECs), forming an in-plane helical configuration. Notably, tangential spin polarization in BiTeI has indeed been reported by spin- and angle-resolved photoemission spectroscopy (spin-ARPES) experiments,[1,4] supporting its description as a prototypical realization of the ideal Rashba system.[16] However, growing theoretical and experimental evidence has suggested that the spin texture in BiTeI can be substantially more complex due to magnetic doping,[17] higher-order Rashba terms allowed by crystal symmetry,[1,18] surface potential variations,[19] spin–orbital entanglement,[20] and site inversion asymmetry associated with the non-centrosymmetric local site point groups, which can generate Dresselhaus-like spin polarization.[21]

A particularly distinctive feature of BiTeI is its

[†] These authors contributed equally to this work.
[‡] Corresponding author. E-mail: ygshi@iphy.ac.cn
[§] Corresponding author. E-mail: xjzhou@iphy.ac.cn
[¶] Corresponding author. E-mail: gdliu_arpes@iphy.ac.cn

© 2026 Chinese Physical Society and IOP Publishing Ltd. All rights, including for text and data mining, AI training, and similar technologies, are reserved.

termination-dependent surface electronic structure. Due to the polar stacking of Te–Bi–I layers, cleavage can produce different local surface terminations, leading to markedly different band bending and Rashba-split surface states.[3,4,22] Recent temperature-dependent photoemission studies have further shown that the surface band bending in layered BiTeI can evolve with temperature, highlighting the pronounced sensitivity of the near-surface electronic structure to local electrostatic and environmental conditions.[23] Scanning tunneling microscopy (STM) studies have revealed that cleaved BiTeI surfaces commonly consist of coexisting tellurium (Te)- and iodine (I)-terminated domains originating from bulk stacking faults, with typical lateral dimensions of only ~ 100 nm.[24–27] Because this termination-relevant length scale is much smaller than the typical beam size in ARPES experiments, the measured spectra inevitably average over many nanoscale domains and therefore reflect a weighted response from termination-dominant or strongly mixed surface regions, rather than from an ideal single-termination surface. Indeed, previous ARPES studies have reported termination-dependent surface electronic structures in BiTeI, including spectra dominated by Te-terminated surface states[1,3,20] as well as spectra containing contributions from mixed Te+I-terminated regions.[4,19] These previous ARPES and STM results provide an important foundation for the surface assignment used in the present work. Nevertheless, although the strong termination dependence of the near-surface electronic structure has been well established, a complete experimental determination of the three-dimensional (3D) spin texture of the Rashba states on different terminations has remained lacking. In particular, whether the actual spin configuration in BiTeI substantially deviates from the ideal tangential Rashba limit has not yet been experimentally resolved, hindering a true understanding of the nature of spin–orbit coupling in it.

Here, for the first time, we directly demonstrate experimentally that the spin texture in BiTeI departs from the ideal Rashba limit in a strongly termination-dependent manner. By performing comprehensive spin-ARPES measurements of the Rashba states along all three orthogonal spin directions (X, Y, Z), we compare the results on a dominant Te-terminated surface with a more strongly mixed Te+I-terminated surface. We find that the Rashba states on the dominant Te-terminated surface remain largely consistent with the conventional Rashba picture as previously reported, with the spin polarization dominated by the expected tangential component. In contrast, the more strongly mixed Te+I-terminated surface exhibits a substantially modified spin configuration characterized not only by the tangential spin polarization, but also by a pronounced radial component and a finite out-of-plane component. It hints that the Dresselhaus effect may play an important role in the SOC-relevant physics of BiTeI. Our results therefore provide direct experimental evidence that the real spin texture of BiTeI is strongly reshaped by the local surface environment, identifying surface termination as a key control parameter for engineering unconventional spin textures in polar Rashba materials.

2. Experiment

Single crystals of BiTeI were grown by the Bridgman method as reported before,[5] with starting compositions of $BiI_3 : Bi : Te = 1 : 2 : 3$. High-purity powders were mixed in a quartz tube in an argon-filled glove box and sealed under high vacuum. The sealed tube was placed in a vertical furnace, first heated to 800 °C to fully melt the sample, then cooled to 600 °C over 24 h. After reaching the target temperature, the quartz tube was pulled toward the low-temperature region at a rate of 1 mm·h^{-1} to obtain single crystals. The ARPES and spin-ARPES measurements were carried out at the BL-9B beamline of the HiSOR of Research Institute for Synchrotron Radiation Science, Hiroshima University, using an R4000 hemispherical electron energy analyzer (Scienta-Omicron).[28–30] Photoelectrons were excited using linear horizontal (LH) polarized light with photon energies of $h\nu = 23$ eV and 25 eV. The energy and angular resolutions for ARPES (spin-ARPES) were set to 37.5 meV (50 meV) and $\sim 0.3^\circ$ ($\sim 1.5^\circ$), respectively. The very low-energy electron diffraction (VLEED)-type spin-polarization detector had a Sherman function of $S = 0.3$. All the samples were cleaved in situ at a low temperature of 15 K and measured in ultra-high vacuum with a base pressure better than 1×10^{-10} mbar. The Fermi level (E_F) is referenced by measuring on a clean polycrystalline gold that is electrically connected to the sample.

3. Results and discussion

To resolve the full 3D spin texture of Rashba-split states in BiTeI, we employed spin-ARPES measurements using the internationally renowned ESPRESSO system at HiSOR.[28–30] As illustrated in Fig. 1(a), the system integrates a hemispherical electron analyzer with two orthogonally arranged very-low-energy electron diffraction (VLEED) spin detectors, enabling simultaneous access to all three spin polarization components (P_X, P_Y, and P_Z). This configuration represents a state-of-the-art and unique realization for 3D spin-polarization vector measurements, overcoming the intrinsic limitations of earlier single-component measurements by combining high efficiency with full spin-vector analysis.

In such measurements, the spin polarization detected in the laboratory frame must be transformed into the intrinsic sample coordinate system when the sample is rotated relative to the detector axis. The geometrical relationship between the measured (P_X, P_Y, P_Z) and intrinsic (P_X^{Sample}, P_Y^{Sample}, P_Z^{Sample})

spin components is schematically shown in Fig. 1(b), where a rotation matrix formalism is applied to reconstruct the true spin vector. Notably, in all spin-resolved measurements, the analyzer slit was aligned to pass through the Γ point, such that the effect of the tilt angle θ can be neglected, and the measured P_Y directly corresponds to the intrinsic P_Y^{Sample}. Furthermore, a detailed geometrical analysis shows that the intrinsic spin components P_X^{Sample} and P_Z^{Sample} can also be directly mapped onto the measured P_X and P_Z. This is because all spin-resolved energy distribution curves (EDCs) in Figs. 2–5 were acquired at emission angles deviating from the sample normal by only a very small angle of $\sim 1^\circ$, for which $\sin\varphi \approx 0$ and $\cos\varphi \approx 1$, leading to $P_X^{\text{Sample}} \approx P_X$ and $P_Z^{\text{Sample}} \approx P_Z$. Therefore, under the present experimental geometry, the measured spin polarization components faithfully represent the intrinsic spin texture of the sample.

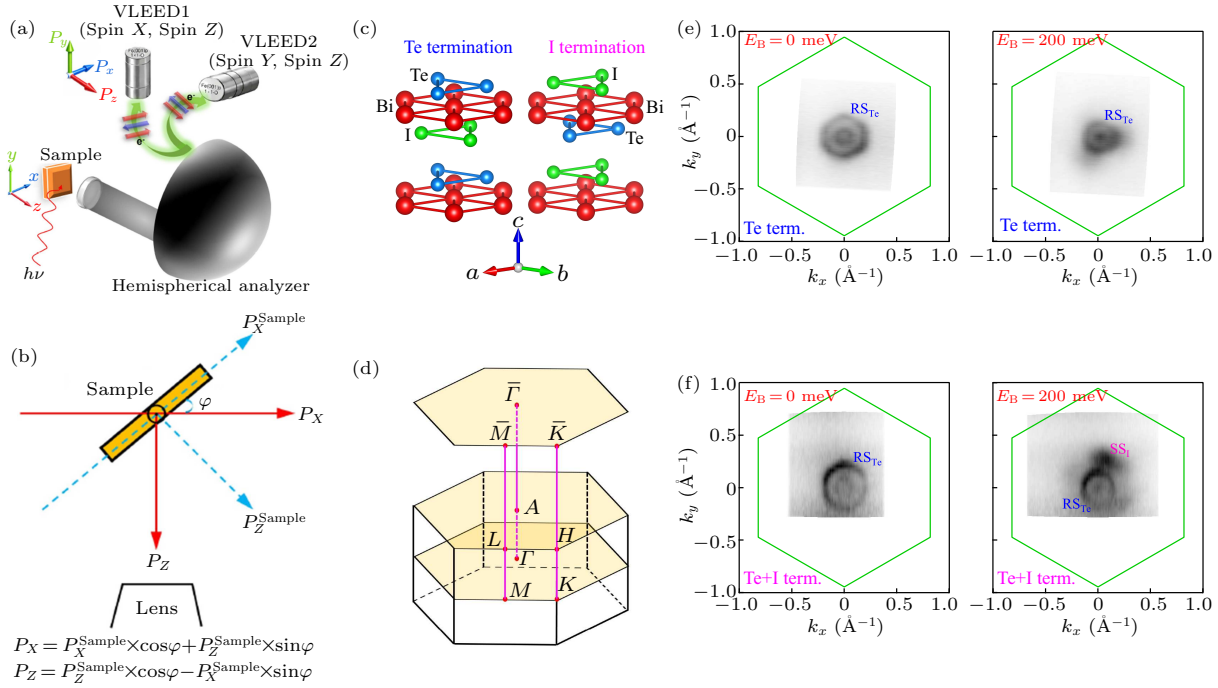


Fig. 1. Spin-resolved ARPES measurements and surface electronic structure of BiTeI. (a) Schematic illustration of the ESPRESSO spin-ARPES system located at HiSOR. The system is equipped with a hemispherical analyzer and two VLEED detectors, enabling simultaneous detection of 3D spin components. (b) Geometrical relationship between the measured spin polarization components (P_X, P_Y, P_Z) in the detector coordinate system and the intrinsic spin polarization (P_X^{Sample}, P_Y^{Sample}, P_Z^{Sample}) in the sample coordinate system when the sample is rotated by an angle φ with respect to the detector axis. The corresponding transformation between the two coordinate systems is illustrated. (c) Two possible cleaving surfaces corresponding to the Te- and I-terminated layers. (d) Schematic plot of the 3D bulk Brillouin zone and its projection onto the (001) surface Brillouin zone. (e) (Left to right) Fermi surface and constant-energy contour at binding energy of 200 meV on the Te-terminated surface, obtained by integrating the spectral intensity within 20 meV with respect to the energy. (f) (Left to right) Fermi surface and constant-energy contour at binding energy of 200 meV on the mixed Te+I-terminated surface, obtained by integrating the spectral intensity within 20 meV with respect to the energy.

BiTeI crystallizes in a trigonal crystal system with space group No. 156 ($P3m1$). The three-dimensional bulk Brillouin zone and its projection onto the (001) surface Brillouin zone are illustrated in Fig. 1(d), with the high-symmetry points marked by red spots. Due to its polar stacking sequence and stacking faults introduced by crystal growth, cleaving can result in distinct surface terminations. As illustrated in Fig. 1(c), two representative terminations are expected: a Te-terminated surface and an I-terminated surface, corresponding to two antiparallel stacking orders. These terminations lead to markedly different surface electronic structures, as clearly manifested in the Fermi surface maps and constant-energy contours (CECs) shown in Figs. 1(e) and 1(f). The Te-terminated surface exhibits well-defined Rashba-split contours (RS_{Te}) with nearly ideal C_3 symmetry, whereas the mixed Te+I-terminated surface gives rise to a pronounced hole-like Fermi pocket (SS_I), indicating modified surface potential and electronic reconstruction. These electron-like Rashba states on the Te-terminated surface and the hole-like surface state on the I-terminated surface have been well established in previous studies through surface-state-resolved density functional theory (DFT) calculations and photon-energy-dependent ARPES measurements.[3,4] In the present measurements, the electron-like Rashba state RS_{Te} shows the inner and outer Fermi wave vectors k_F of $\sim$0.07 Å^{-1} and $\sim$0.19 Å^{-1}, respectively, with a band bottom located at about 0.4 eV below the E_F. These values are consistent with those reported previously for the electron-like Rashba surface states on the Te-terminated surface.[3,4,20] For the hole-like surface state SS_I, the extracted momenta are approximately 0.32 Å^{-1} and 0.40 Å^{-1} at binding energies of 0.3 eV and 0.4 eV, respectively, also in good agreement with the previous ARPES results for the I-terminated

surface.[3,4] The reliable identification of these surface states provides a solid foundation for the spin-resolved ARPES investigations on different surface terminations presented below.

We first examine the spin texture of the Rashba-split states on the dominant Te-terminated surface. For convenience, we hereafter refer to such surfaces simply as the Te-terminated surface. Figures 2 and 3 present spin-resolved measurements along the $\bar{\Gamma}$–$\bar{M}$ and $\bar{\Gamma}$–$\bar{K}$ high-symmetry directions, respectively. The spin-integrated band dispersions (Figs. 2(b) and 3(b)) reveal the characteristic Rashba splitting, with two branches dispersing away from the zone center. The corresponding spin-resolved EDCs at selected momentum points (P1–P3) demonstrate a dominant spin polarization along the tangential direction (P_Y), reaching values up to ∼70%, and exhibiting a pronounced sign reversal between the inner and outer Rashba-split bands (Figs. 2(d), 2(g), 2(j) and 3(d), 3(g), 3(j)). In addition to the tangential component, a weak radial spin polarization (P_X) is also resolved on the Te-terminated surface (Figs. 2(e), 2(h), 2(k) and 3(e), 3(h), 3(k)), which remains much smaller than the tangential component. Notably, at the same momentum points, the P_X component exhibits a clear sign reversal between the EDC peaks at lower and higher binding energies, which correspond to the inner and outer Rashba-split branches, respectively. Meanwhile, the out-of-plane component (P_Z) remains negligible within the experimental resolution (Figs. 2(f), 2(i), 2(l) and 3(f), 3(i), 3(l)). These results demonstrate that the spin texture on the Te-terminated surface (Figs. 2(c) and 3(c)) closely follows the ideal in-plane helical configuration of the Rashba model, with a dominant tangential spin component (P_Y). Such behavior is in good agreement with previous spin-ARPES studies reporting predominantly tangential spin polarization.[1,4,19]

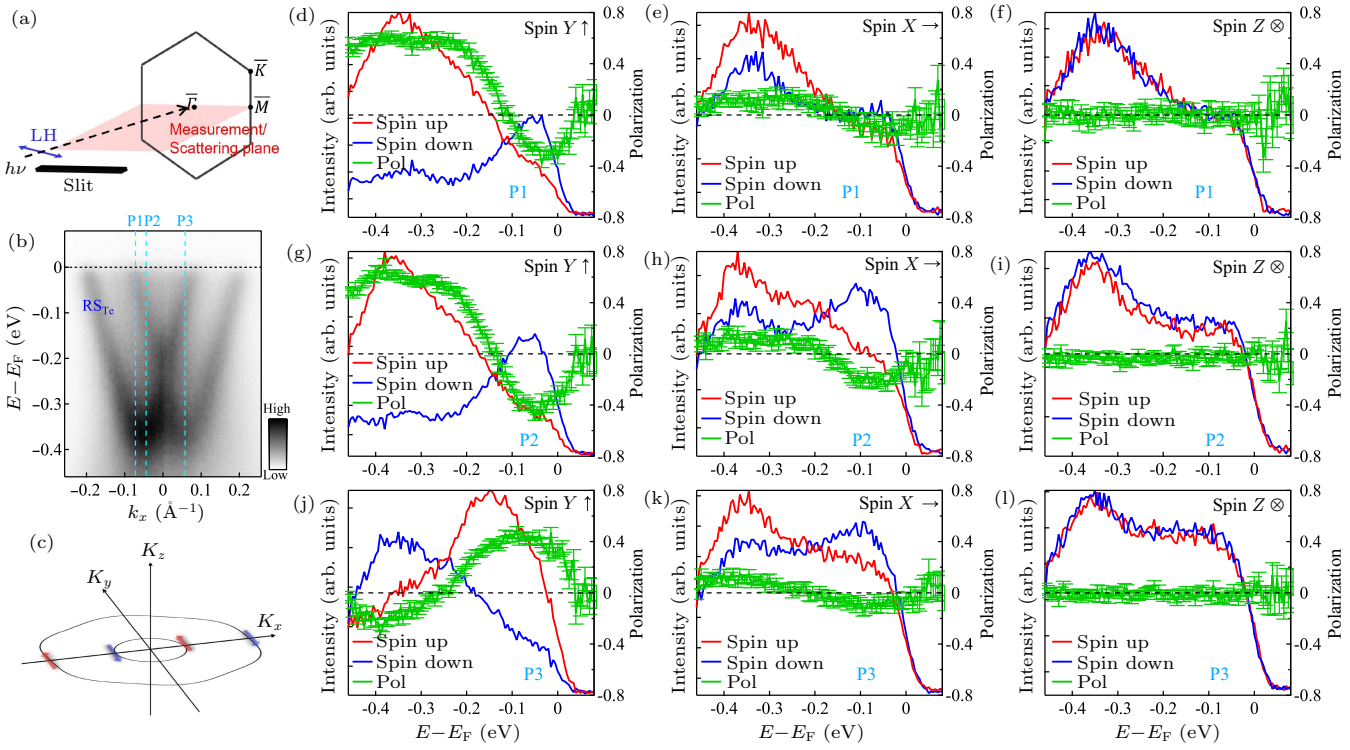


Fig. 2. 3D spin vector measurement of the Rashba state along the $\bar{\Gamma}$–$\bar{M}$ direction on the Te-terminated surface of BiTeI. (a) Experimental geometry illustrating the measurement configuration, including the polarization of light, the light incidence, analyzer slit direction, and the measurement (scattering) plane relative to the surface Brillouin zone. (b) Spin-integrated ARPES intensity map along the $\bar{\Gamma}$–$\bar{M}$ high-symmetry direction. Three representative momentum points (P1, P2, and P3) used for spin-resolved EDCs measurements (d)–(l) are marked by blue dashed lines. (c) Schematic illustration of the spin textures of the inner and outer Rashba-split branches. (d)–(f) Spin-resolved EDCs at P1 for the spin-*y*, spin-*x*, and spin-*z* components in the detector coordinate system. The red and blue curves represent spin-up and spin-down intensities, respectively, while the green symbols denote the corresponding spin polarization. (g–i) Same as (d–f), but at P2. (j)–(l) Same as (d)–(f), but at P3. The data in panels (a)–(l) were acquired at 15 K by using spin-ARPES with a photon energy of 23 eV.

In striking contrast, the spin texture on the mixed Te+I-terminated surface exhibits pronounced deviations from the ideal Rashba picture.[16] As shown in Figs. 4 and 5, the Rashba-split bands along both $\bar{\Gamma}$–$\bar{M}$ and $\bar{\Gamma}$–$\bar{K}$ directions display substantial radial spin polarization (P_X) ∼40%, in some momentum positions becoming comparable in magnitude to the tangential component (P_Y) (Figs. 4(k) and 5(k)). This indicates a strong reconstruction of the in-plane spin texture. Even more remarkably, a sizable out-of-plane spin component (P_Z) emerges on the mixed Te+I-terminated surface, particularly on the inner Rashba branch (Figs. 4(i), 4(l) and 5(i), 5(l)). This behavior is absent on the Te-terminated surface and represents a clear signature of spin reorientation beyond a purely in-plane configuration. The coexistence of significant P_X, P_Y, and P_Z components demonstrates that the spin texture evolves into a fully three-dimensional configuration.

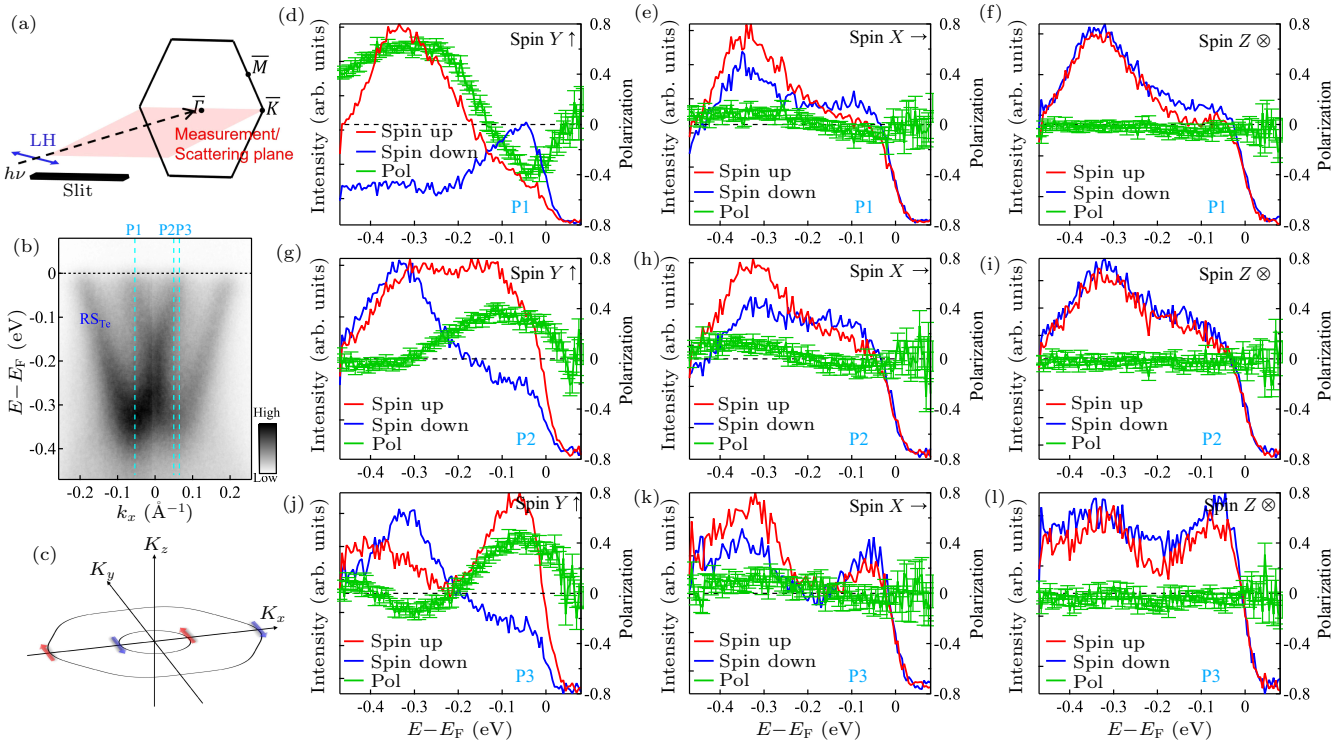


Fig. 3. 3D spin vector measurement of the Rashba state along the $\bar{\Gamma}$–$\bar{K}$ direction on the Te-terminated surface of BiTeI. (a) Experimental geometry illustrating the measurement configuration, including the polarization of light, the light incidence, analyzer slit direction, and the measurement (scattering) plane relative to the surface Brillouin zone. (b) Spin-integrated ARPES intensity map along the $\bar{\Gamma}$–$\bar{K}$ high-symmetry direction. Three representative momentum points (P1, P2, and P3) used for spin-resolved EDCs measurements (d)–(l) are marked by blue dashed lines. (c) Schematic illustration of the spin textures of the inner and outer Rashba-split branches. (d)–(f) Spin-resolved EDCs at P1 for the spin-*y*, spin-*x*, and spin-*z* components in the detector coordinate system. The red and blue curves represent spin-up and spin-down intensities, respectively, while the green symbols denote the corresponding spin polarization. (g)–(i) Same as (d)–(f), but at P2. (j)–(l) Same as (d)–(f), but at P3. The data in panels (a)–(l) were acquired at 15 K by using spin-ARPES with a photon energy of 23 eV.

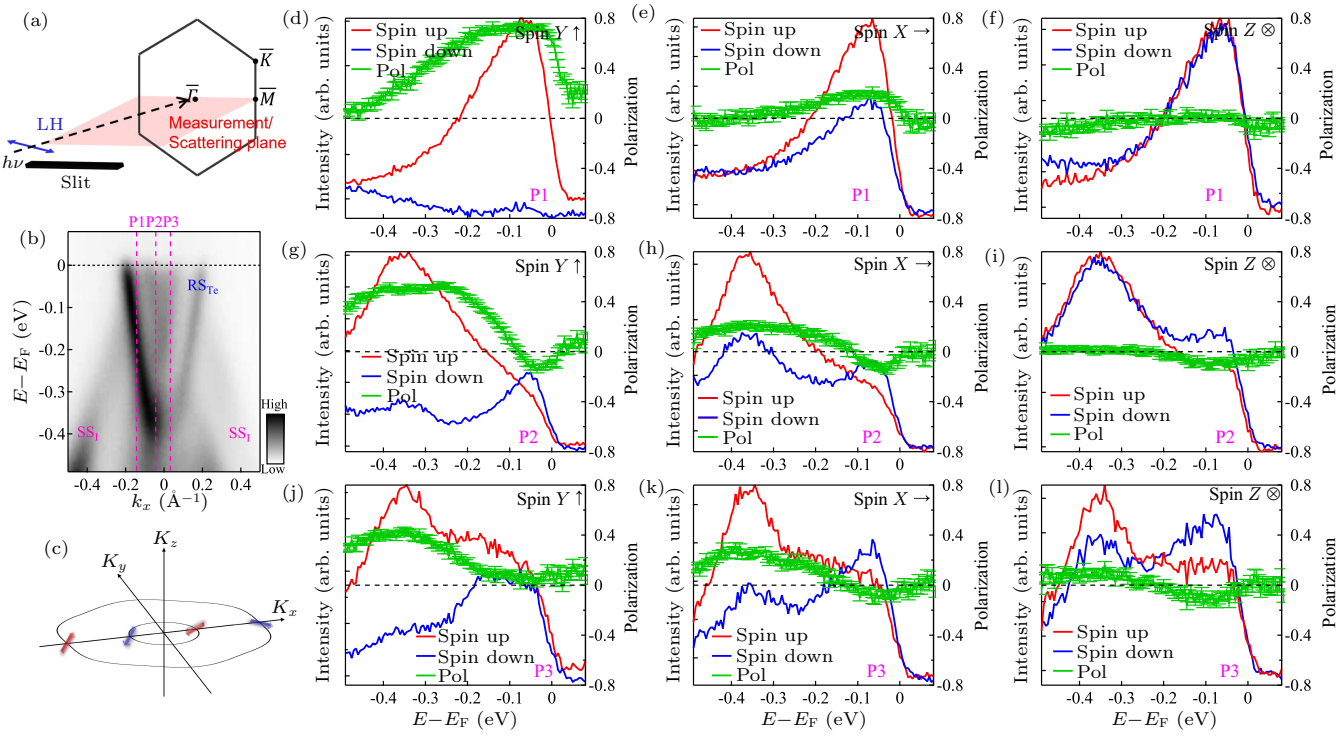


Fig. 4. 3D spin vector measurement of the Rashba state along the $\bar{\Gamma}$–$\bar{M}$ direction on the mixed Te+I-terminated surface of BiTeI. (a) Experimental geometry illustrating the measurement configuration, including the polarization of light, the light incidence, analyzer slit direction, and the measurement (scattering) plane relative to the surface Brillouin zone. (b) Spin-integrated ARPES intensity map along the $\bar{\Gamma}$–$\bar{M}$ high-symmetry direction. Three representative momentum points (P1, P2, and P3) used for spin-resolved EDCs measurements (d)–(l) are marked by pink dashed lines. (c) Schematic illustration of the spin textures of the inner and outer Rashba-split branches. (d)–(f) Spin-resolved EDCs at P1 for the spin-*y*, spin-*x*, and spin-*z* components in the detector coordinate system. The red and blue curves represent spin-up and spin-down intensities, respectively, while the green symbols denote the corresponding spin polarization. (g)–(i) Same as (d)–(f), but at P2. (j)–(l) Same as (d)–(f), but at P3. The data in panels (a)–(l) were acquired at 15 K by using spin-ARPES with a photon energy of 25 eV.

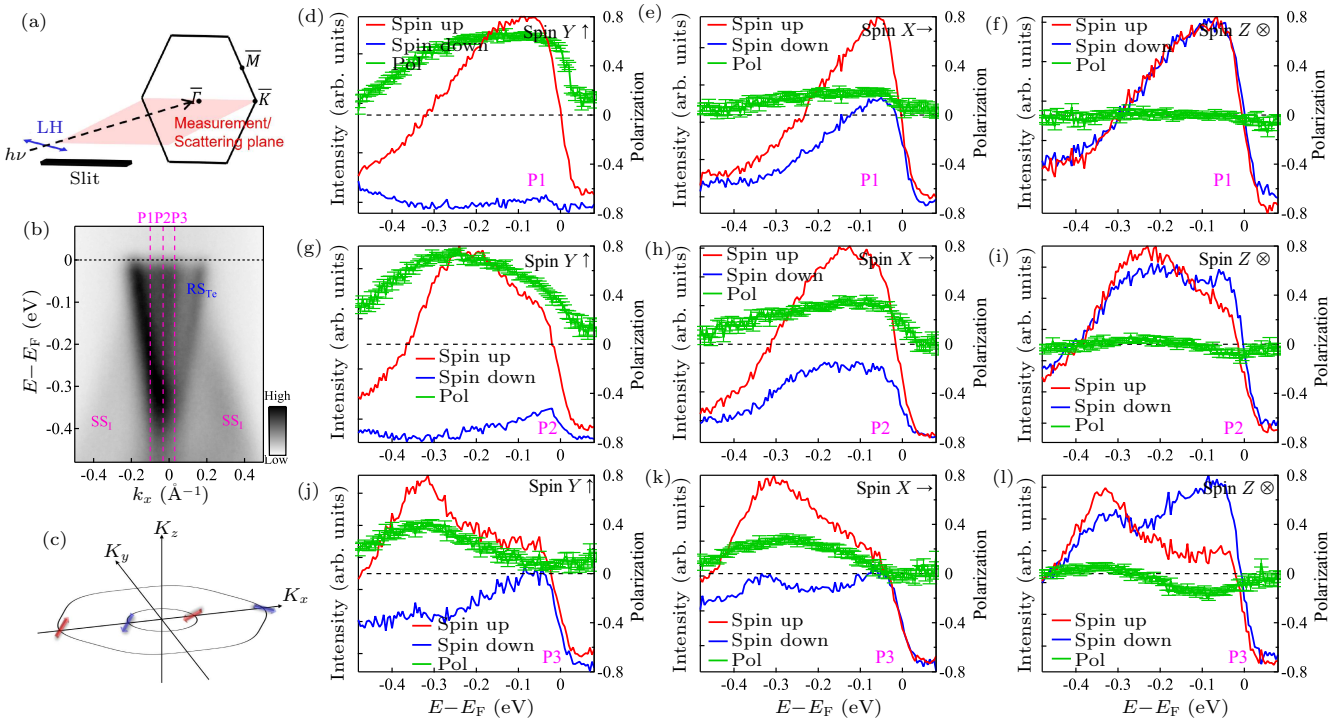


Fig. 5. 3D spin vector measurement of the Rashba state along the $\bar{\Gamma}$–$\bar{K}$ direction on the mixed Te+I-terminated surface of BiTeI. (a) Experimental geometry illustrating the measurement configuration, including the polarization of light, the light incidence, analyzer slit direction, and the measurement (scattering) plane relative to the surface Brillouin zone. (b) Spin-integrated ARPES intensity map along the $\bar{\Gamma}$–$\bar{K}$ high-symmetry direction. Three representative momentum points (P1, P2, and P3) used for spin-resolved EDCs measurements (d)–(l) are marked by pink dashed lines. (c) Schematic illustration of the spin textures of the inner and outer Rashba-split branches. (d)–(f) Spin-resolved EDCs at P1 for the spin-*y*, spin-*x*, and spin-*z* components in the detector coordinate system. The red and blue curves represent spin-up and spin-down intensities, respectively, while the green symbols denote the corresponding spin polarization. (g)–(i) Same as (d)–(f), but at P2. (j)–(l) Same as (d)–(f), but at P3. The data in panels (a)–(l) were acquired at 15 K by using spin-ARPES with a photon energy of 25 eV.

These results establish the full three-dimensional spin-vector information of the Rashba-split states for the two surface terminations of BiTeI and reveal a spin texture that deviates markedly from the ideal Rashba limit, particularly on the surface where a clearly resolved I-derived hole-like surface band (SS_I) is present.

The observed deviation from the ideal Rashba spin texture raises important questions regarding its microscopic origin. First, on the mixed Te+I-terminated surface we observe a pronounced radial spin component (spin *X*), i.e., a spin component parallel to the crystal momentum. In contrast to the ideal Rashba picture, our high-resolution spin-ARPES measurements impose a stricter, branch-resolved constraint: the radial spin polarization exhibits a clear sign reversal between the inner and outer Rashba-split bands. Notably, this effect is particularly pronounced in the mixed Te+I termination, where a well-resolved hole-like valence surface state (SS_I) is present, in which case the radial spin polarization can reach values as high as ∼40%. A comparison between the nearly pure Te-terminated surface and the mixed Te+I termination reveals that the radial spin polarization becomes substantially enhanced with clear I contribution at the surface, as evidenced by observation of the I-derived surface state SS_I. Therefore, we attribute the observed unconventional spin texture of the Te+I-terminated surface states to the contribution of the hole-like surface state SS_I associated with the I termination, whose genuine spin polarization has not yet been investigated. It is noted that the previous work by Maaß *et al*. reported only the spin component parallel to the *Y* direction,[19] while the remaining spin components were not resolved in the I-containing cleaving surface.

The microscopic mechanism of the unconventional spin texture associated with the hole-like surface state on the I-terminated surface of BiTeI may involve several, not mutually exclusive, mechanisms. First, because BiTeI belongs to the C_{3v} point group, higher-order Rashba terms allowed by crystal symmetry can, in principle, drive deviations from the ideal purely tangential Rashba helicity and give rise to additional nontrivial spin components.[1,18,31] Indeed, recent studies on related BiTeCl Rashba semiconductors have further revealed higher-order-Rashba-induced spin-texture reconstruction,[32] highlighting the importance of going beyond the ideal Rashba model. More generally, the effective-Hamiltonian studies of non-centrosymmetric two-dimensional systems have shown that the Rashba SOC can coexist with the momentum-dependent higher-order SOC terms, which tend to pin spins along the out-of-plane direction and thus emphasize the broader importance of the momentum-dependent SOC contributions beyond the conventional Rashba picture.[33] Second, from the viewpoint that spin polarization

is fundamentally governed by local site asymmetry rather than solely by global crystal symmetry, BiTeI has been theoretically predicted to host intertwined Rashba- and Dresselhaus-like spin orbital interaction.[21] In this scenario, the I atomic layer, which is characterized by a crystal-field environment distinct from that of the Te atomic layer (the inequivalent Bi–I and Bi–Te bond lengths and electronegativities), can exhibit a modified near-surface local symmetry. In particular, the basic structural unit of the [I–Bi–Te] trilayer breaks spatial inversion symmetry, thus satisfying the Dresselhaus condition. More importantly, based on the comparison between the 3D spin textures measured on the two terminations, the contribution of this possible Dresselhaus effect is a unique property of the valence band, and the hole-like surface state on the I-terminated surface clearly originates from the bulk valence band; in contrast, the electron-type surface state on the Te-terminated surface originates from the conduction band, making it practically impossible to observe such unconventional spin texture. A sizable out-of-plane spin component observed in the inner Rashba-split band provides additional support for the Dresselhaus-like scenario. This consideration is also consistent with previous studies, showing that the electronic structure of BiTeI is highly sensitive to local structural details: small variations in the Bi–Te and Bi–I interlayer distances can substantially modify the calculated band structure and Fermi-surface topology,[34] while the annealing-induced changes in near-surface stoichiometry and atomic stacking can strongly reconstruct the surface electronic structure and even induce topological surface states with helical spin texture.[35] Third, the enhanced radial and out-of-plane spin texture on the I-rich surface may be closely related to the local electrostatic environment of the I termination. In the ideal Rashba picture, the potential gradient is dominated by the surface-normal component, giving rise to a tangential in-plane helical spin texture. However, for the I-terminated surface of BiTeI, the exposed iodine layer is negatively charged and highly electronegative, resulting in a polar ionic coupling between the $(BiTe)^+$ and I^- layers,[25] as well as a surface-modified local crystal-field environment for the near-surface states. As a result, the microscopic potential gradient experienced by these states may deviate from a purely out-of-plane form and contain atomic-scale in-plane components. In the general form $H_{SOC} \propto \sigma \cdot (\nabla V \times \boldsymbol{k})$, such local in-plane components of ∇V can effectively tilt the Rashba vector. Notably, this view is further supported by a closely related calculation on the sister compound BiTeCl, which showed that, compared with the Te-terminated surface, the Cl-terminated surface exhibits an unconventional spin texture owing to a larger in-plane potential gradient, in particular showing a pronounced out-of-plane spin component.[36] Fourth, this unconventional spin texture may be further related to the orbital sensitivity of the Rashba coupling in BiTeI. Previous theoretical studies have shown that the relative energy alignment between the out-of-plane p_z-dominated states and the in-plane p_{xy}-derived states is a key microscopic parameter controlling the symmetry-allowed coupling between the lowest conduction band and the highest valence band.[37,38] The distinct local electrostatic potential and crystal-field environment at the I-terminated surface may therefore shift these orbital components in energy relative to each other and change their hybridization, providing a plausible route from a standard tangential Rashba texture to the radial and out-of-plane spin texture pattern observed here.

Our present results do not yet allow us to unambiguously disentangle these effects, and it is also possible that the observed unconventional spin texture reflects their cooperative interplay on the I-terminated surface. Further investigation will require a more definitive separation of the spin-polarization signal associated with the pure I-terminated surface, by employing a sub-micro spatial-resolved and 3D spin-ARPES technique, although being hard to realize. Considering the van-der-Waals-like layered structure, the spin–orbital interaction on the surface stems from that existing in the bulk; it is therefore expected that the bulk valence band may also hold a similar unconventional spin texture as on the iodine-terminated surface. On the theoretical side, the surface-state-resolved band calculations that explicitly incorporate the I termination, realistic near-surface structural relaxation, as well as termination-dependent potential gradients and orbital hybridization, will be highly desirable. Such combined experimental and theoretical efforts should provide a more decisive answer on the underlying mechanism.

Taken together, our results report the first unambiguous, band-resolved determination of the full 3D spin-vector texture for both the inner and outer Rashba-split states in BiTeI. By directly resolving all three spin components (P_X, P_Y, and P_Z) with high precision, our study goes beyond the long-standing limitation of partial spin detection in a single Rashba branch and establishes a stringent experimental benchmark for understanding unconventional spin textures in this outstanding material and the related spin–orbit-coupled systems. More importantly, the pronounced evolution of the spin texture with surface termination reveals that the spin configuration is not an immutable property but can be fundamentally reconfigured through surface engineering. This identifies surface termination as a powerful and previously underappreciated control knob for tailoring spin textures of materials. This conclusion also resonates with recent progress in spin-texture engineering in magnetic and spin–orbit-coupled systems, where real-space topological spin textures can be tuned by electric-field, interfacial, or symmetry design and indirectly probed through the magneto-transport or magneto-optical responses.[39,40] Our findings not only advance the microscopic understanding of

spin–momentum locking beyond the ideal Rashba paradigm in BiTeI but also provide a clear design principle for achieving controllable spin functionalities, paving the way toward its high-performance low-dimensional spintronic device applications.

4. Summary

In summary, we have experimentally resolved the full 3D spin texture of Rashba-split states in BiTeI using high-resolution spin-ARPES, achieving for the first time a branch-resolved determination of the complete spin configuration for both the inner and outer Rashba-split, going beyond previous spin-ARPES studies that were mainly limited to the in-plane tangential spin polarization. While the Te-terminated surface largely preserves the canonical Rashba picture with dominant tangential spin polarization, the mixed Te+I-terminated surface exhibits a pronounced reconstruction of the spin texture, manifested by substantial radial and appreciable out-of-plane spin components. The strong correlation between this unconventional spin configuration and the emergence of the I-derived hole-like surface state suggests that the spin–momentum locking in BiTeI is not solely governed by the ideal Rashba mechanism, but is strongly reshaped by the local surface potential and termination-dependent symmetry environment, likely associated with Dresselhaus-like spin polarization arising from site inversion asymmetry in the non-centrosymmetric local site point groups and higher-order Rashba effects. These findings establish BiTeI as a platform in which Rashba spin textures can be fundamentally reconfigured by surface termination, revealing surface engineering as an effective route to tailor 3D spin configurations in polar spin–orbit-coupled materials. Our results therefore advance the microscopic understanding of spin–momentum locking beyond the ideal Rashba paradigm and provide a design principle for realizing controllable spin functionalities in low-dimensional spintronic devices.

Acknowledgements

This work is supported by the National Key Research and Development Program of China (Grants Nos. 2022YFA1403901 and 2023YFA1406103 by G.D.L., 2024YFA1408400 by Y.G.S., and 2022YFA1604200 by L.Z), the National Natural Science Foundation of China (Grant Nos. 12488201 by X.J.Z., 12374066 by L.Z., and U22A6005 by Y.G.S), and the Synergetic Extreme Condition User Facility (SECUF, https://cstr.cn/31123.02.SECUF). Synchrotron ARPES measurements at HiSOR were performed under the approval of the Program Advisory Committee (Proposal Numbers: 22BG045 and 23AG023).

References

[1] Ishizaka K, Bahramy M S, Murakawa H, Sakano M, Shimojima T, Sonobe T, Koizumi K, Shin S, Miyahara H, Kimura A, Miyamoto K, Okuda T, Namatame H, Taniguchi M, Arita R, Nagaosa N, Kobayashi K, Murakami Y, Kumai R, Kaneko Y, Onose Y and Tokura Y 2011 *Nat. Mater.* **10** 521

[2] Sakano M, Miyawaki J, Chainani A, Takata Y, Sonobe T, Shimojima T, Oura M, Shin S, Bahramy M S, Arita R, Nagaosa N, Murakawa H, Kaneko Y, Tokura Y and Ishizaka K 2012 *Phys. Rev. B* **86** 085204

[3] Crepaldi A, Moreschini L, Autès G, Tournier-Colletta C, Moser S, Virk N, Berger H, Bugnon Ph, Chang Y J, Kern K, Bostwick A, Rotenberg E, Yazyev O V and Grioni M 2012 *Phys. Rev. Lett.* **109** 096803

[4] Landolt G, Eremeev S V, Koroteev Y M, Slomski B, Muff S, Neupert T, Kobayashi M, Strocov V N, Schmitt T, Aliev Z S, Babanly M B, Amiraslanov I R, Chulkov E V, Osterwalder J and Dil J H 2012 *Phys. Rev. Lett.* **109** 116403

[5] Cai L, Yu C, Zhao W, Li Y, Feng H, Zhou H A, Wang L, Zhang X, Zhang Y, Shi Y, Zhang J, Yang L and Jiang W 2022 *Nano Lett.* **22** 7441

[6] Li X, Fu Z, He Y, Yu X, Yang Y and Li W 2023 *Appl. Phys. Lett.* **122** 112405

[7] Zhang P, Zhou Z, Hu S, Gao H and Wang Y 2022 *J. Appl. Phys.* **132** 203903

[8] Fülöp B, Tajkov Z, Pető J, Kun P, Koltai J, Oroszlány L, Tóvári E, Murakawa H, Tokura Y, Bordács S, Tapasztó L and Csonka S 2018 *2D Mater.* **5** 031013

[9] Antonatos N, Kovalska E, Mazánek V, Veselý M, Sedmidubský D, Wu B and Sofer Z 2021 *ACS Appl. Nano Mater.* **4** 590

[10] Bianca G, Trovatello C, Zilli A, Zappia M I, Bellani S, Curreli N, Conticello I, Buha J, Piccinni M, Ghini M, Celebrano M, Finazzi M, Kriegel I, Antonatos N, Sofer Z and Bonaccorso F 2022 *ACS Appl. Mater. Interfaces* **14** 34963

[11] Petrini N, Asaithambi A, Rebecchi L and Curreli N 2023 *Opt. Mater. X* **19** 100255

[12] Kang R, Ge J F, He Y, Zhu Z, Larson D T, Saghir M, Hoffman J D, Balakrishnan G and Hoffman J E 2024 arXiv:2402.18779

[13] Kwock K W C, Norden T, Darlington T P, Yao K, Du K, Nedić A M, Trevisan T V, Dolgopolova E, Orth P P, Prasankumar R P, Schuck P J, Cheong S W, Kort-Kamp W J M and Padmanabhan P 2026 arXiv:2601.00195

[14] Li Y, Wu C, Sun X, Ye L, Lu Y, Lin H Q, Duan W and Huang B 2026 *Newton* **2** 100368

[15] Bychkov Yu A and Rashba É I 1984 *JETP lett.* **39** 78

[16] Rashba E I 1960 *Sov. Phys.-Solid State* **2** 1109

[17] Shikin A M, Rybkina A A, Klimovskikh I I, Tereshchenko O E, Bogomyakov A S, Kokh K A, Kimura A, Skirdkov P N, Zvezdin K A and Zvezdin A K 2017 *2D Mater.* **4** 025055

[18] Bahramy M S, Yang B J, Arita R and Nagaosa N 2012 *Nat. Commun.* **3** 679

[19] Maaß H, Bentmann H, Seibel C, Tusche C, Eremeev S V, Peixoto T R F, Tereshchenko O E, Kokh K A, Chulkov E V, Kirschner J and Reinert F 2016 *Nat. Commun.* **7** 11621

[20] Bawden L, Riley J M, Kim C H, Sankar R, Monkman E J, Shai D E, Wei H I, Lochocki E B, Wells J W, Meevasana W, Kim T K, Hoesch M, Ohtsubo Y, Le Fèvre P, Fennie C J, Shen K M, Chou F and King P D C 2015 *Sci. Adv.* **1** e1500495

[21] Zhang X, Liu Q, Luo J W, Freeman A J and Zunger A 2014 *Nat. Phys.* **10** 387

[22] Sakano M, Bahramy M S, Katayama A, Shimojima T, Murakawa H, Kaneko Y, Malaeb W, Shin S, Ono K, Kumigashira H, Arita R, Nagaosa N, Hwang H Y, Tokura Y and Ishizaka K 2013 *Phys. Rev. Lett.* **110** 107204

[23] Yan H, Shi D, Dong J, Ou T, Liu Z, Liu Y, Sun Z and Chen Z 2025 *J. Phys. Chem. C* **129** 9051

[24] Tournier-Colletta C, Autès G, Kierren B, Bugnon Ph, Berger H, Fagot-Revurat Y, Yazyev O V, Grioni M and Malterre D 2014 *Phys. Rev. B* **89** 085402

[25] Butler C J, Yang H H, Hong J Y, Hsu S H, Sankar R, Lu C I, Lu H Y, Ou Yang K H, Shiu H W, Chen C H, Kaun C C, Shu G J, Chou F C and Lin M T 2014 *Nat. Commun.* **5** 4066

[26] Fiedler S, El-Kareh L, Eremeev S V, Tereshchenko O E, Seibel C, Lutz P, Kokh K A, Chulkov E V, Kuznetsova T V, Grebennikov V I, Bentmann H, Bode M and Reinert F 2014 *New J. Phys.* **16** 075013

[27] Fiedler S, Bathon T, Eremeev S V, Tereshchenko O E, Kokh K A, Chulkov E V, Sessi P, Bentmann H, Bode M and Reinert F 2015 *Phys. Rev. B* **92** 235430
[28] Okuda T, Miyamoto K, Miyahara H, Kuroda K, Kimura A, Namatame H and Taniguchi M 2011 *Rev. Sci. Instrum.* **82** 103302
[29] Okuda T, Miyamoto K, Kimura A, Namatame H and Taniguchi M 2015 *J. Electron Spectrosc. Relat. Phenom.* **201** 23
[30] Okuda T 2017 *J. Phys.: Condens. Matter* **29** 483001
[31] Vajna Sz, Simon E, Szilva A, Palotas K, Ujfalussy B and Szunyogh L 2012 *Phys. Rev. B* **85** 075404
[32] Qu J, Han X, Sakamoto S, Jia C J, Liu J, Li H, Guan D, Zeng Y J, Schüler M, Kirchmann P S, Moritz B, Hussain Z, Devereaux T P, Shen Z X and Sobota J A 2023 *npj Quantum Mater* **8** 13
[33] Yu S B, Zhou M, Zhang D and Chang K 2021 *Phys. Rev. B* **104** 075435
[34] Kuibarov A, Fedorov A, Bezguba V, Berger H, Yaresko A, Voroshnin V, Kordyuk A, Baumgärtel P, Büchner B and Borisenko S 2022 *Phys. Rev. B* **105** 235112
[35] Fiedler S, Eremeev S V, Golyashov V A, Kaveev A K, Tereshchenko O E, Kokh K A, Chulkov E V, Bentmann H and Reinert F 2018 *New J. Phys.* **20** 063035
[36] Eremeev S V, Nechaev I A, Koroteev Yu M, Echenique P M and Chulkov E V 2012 *Phys. Rev. Lett.* **108** 246802
[37] Bahramy M S, Arita R and Nagaosa N 2011 *Phys. Rev. B* **84** 041202(R)
[38] Bahramy M S and Ogawa N 2017 *Adv. Mater.* **29** 1605911
[39] Liu X, Zhang D, Deng Y, Jiang N, Zhang E, Shen C, Chang K and Wang K 2024 *ACS Nano* **18** 1013
[40] Lu Y, Zhang D and Chang K 2025 *Chin. Phys. Lett.* **42** 057402